Ceramics International xxx (xxxx) xxx

Contents lists available at ScienceDirect

Ceramics International

journal homepage: www.elsevier.com/locate/ceramint

«Ellestadite»-type anionic $[PO_4]^{3-} \rightarrow [SO_4]^{2-}$ substitutions in β-$Ca_3(PO_4)_2$ type compounds: A new route to design the inorganic phosphors

Dina V. Deyneko [a,b,*], Vladimir V. Titkov [a], Fedor D. Fedyunin [c], Dmitry A. Spassky [d,e], Sergey N. Volkov [b], Elena Yu. Borovikova [f,g], Bogdan I. Lazoryak [a], Sergey M. Aksenov [b,h]

[a] Department of Chemistry, Lomonosov Moscow State University, 119991, Moscow, Russia
[b] Laboratory of Arctic Mineralogy and Material Sciences, Kola Science Centre, Russian Academy of Sciences, 14 Fersman Str., Apatity, 184209, Russia
[c] Physics Department, Lomonosov Moscow State University, 119991, Moscow, Russia
[d] Skobeltsyn Institute of Nuclear Physics, Moscow State University, Leninskiye Gory 1-2, 11991, Moscow, Russia
[e] Institute of Physics, University of Tartu, W. Ostwaldi Street 1, 50411, Tartu, Estonia
[f] Geology Department, Lomonosov Moscow State University, 119991, Moscow, Russia
[g] Laboratory of Nature-Inspired Technologies and Environmental Safety of the Arctic, Kola Science Centre, Russian Academy of Sciences, 14 Fersman Street, Apatity, 184209, Russia
[h] Geological Institute, Kola Science Centre, Russian Academy of Sciences, 14 Fersman Street, Apatity, 184209, Russia

ARTICLE INFO

Keywords:
Crystal structure
Phosphates
Sulfates
Mixed salts
Anionic substitution
Photoluminescence
Tricalcium phosphate
Inorganic phosphors
Optical materials

ABSTRACT

Sulfate anion plays an important role in the development of inorganic phosphors and is considered as the path for for the enhancement of the luminescent properties. The heterovalent $[PO_4]^{3-} \rightarrow [SO_4]^{2-}$ anion substitution in the β-$Ca_3(PO_4)_2$-type compounds was realized using the "ellestadite"-type strategy called by the analogy with the apatite-type structures. The novel compounds belonging to the $Ca_{10.5-0.5x-y}M_y(PO_4)_{7-x}(SO_4)_x$, M = Ca^{2+}, Mg^{2+} and Zn^{2+} series have been synthesized using high-temperature solid state reaction. The used isomorphous scheme was $[PO_4]^{3-} + ½\ Ca^{2+} = [SO_4]^{2-} + ½\ \square$ with the formation of the vacancy for the charge compensation. The successful incorporation of $[SO_4]^{2-}$ groups was approved by Fourier-transform infrared spectroscopy, EDX method, and powder X-ray diffraction analysis. It was found that the sulfur atoms predominantly occupied T2 sites in the anionic sublattice according to crystal structure refinement based on the analysis of interatomic distances. The photoluminescent properties were studied for the Eu^{3+}-doped samples and it was shown that Zn^{2+}-containing samples exhibit a 1.5 times higher intensity in comparison with Mg^{2+}-containing substituted phosphates. Thus, a new "ellestadite"-type substitution in β-$Ca_3(PO_4)_2$-type structure significantly expands the crystal chemistry and give more insights into the deeper understanding of the dependence of luminescent properties on the cation distribution. The pathways of the $[SO_4]^{2-}$ incorporation into the crystal structures are discussed in details.

1. Introduction

Among oxysalt inorganic phosphors, which are considered as the most promising host-matrices based on or derived from calcium phosphates, form a considerably large family of materials which is extensively studied. These materials are predominantly characterized by one of two structural types: apatite or β-$Ca_3(PO_4)_2$ (which is synthetic analog of natural mineral whitlockite). The general formula of compounds with the apatite-type structure is $^{[9]}A1_4\ ^{[7]}A2_6[\ ^{[4]}XO_4]_6Y_2$ [1]. In natural samples *A* site can be occupied by monovalent (Na^+), divalent (Ca^{2+}, Pb^{2+}, Ba^{2+}, Sr^{2+}, Mn^{2+}), and trivalent (Ce^{3+}, La^{3+}, Y^{3+}, Bi^{3+}) ions; *X* = P^{5+}, As^{5+}, V^{5+}, Si^{4+}, S^{6+}, B^{3+}; *Y* = F^-, Cl^-, OH^-. The general formula of compounds with the β-$Ca_3(PO_4)_2$-type structure is $Ca_{10.5-0.5(x-2y-3z)}A^+_xB^{2+}_yR^{3+}_z(TO_4)_7$, where *A* – monovalent alkaline cations (Li^+, Na^+, K^+); B^{2+} – alkaline-earth divalent cations (Ca^{2+}, Sr^{2+}) and cations of transition 3d-metals (Cu^{2+}, Zn^{2+}, Fe^{2+}, Ni^{2+}); R^{3+} – rare-earth REE^{3+} elements (Y^{3+} Sc^{3+}, Ln^{3+}), as well as Bi^{3+}, Cr^{3+}, Al^{3+}, In^{3+}; *T* – tetrahedral cations – P^{5+}, V^{5+}. Due to wide range of isomorphous substitutions within the initial host-matrix, it is possible to modify the crystal structure by varying the cationic and anionic sites to design novel materials with the directly improved physical properties.

It was previously shown that anionic tetrahedral substitutions make

* Corresponding author. Chemistry Department, Moscow State University, Leninskie Gory 1, 119991, Moscow, Russia.
E-mail address: deynekomsu@gmail.com (D.V. Deyneko).

https://doi.org/10.1016/j.ceramint.2022.05.077
Received 31 March 2022; Received in revised form 27 April 2022; Accepted 6 May 2022
Available online 11 May 2022

a significant contribution to the luminescent properties of compounds both with apatite [2–4] and β-$Ca_3(PO_4)_2$ [5–7] type structures. The preservation of the structural types is controlled by the similar size (in particular, bond distances), coordinational environment and geometry as well as the stereoactivity of the $[PO_4]^{3-}$-tetrahedral phosphate anion and the substituted $[XO_4]^{n-}$-tetrahedron, *e.g.* despite the different negative charges, the covalent character of the bonds in $[PO_4]^{3-}$ tetrahedral anion is similar to those in aluminate $[AlO_4]^{5-}$, silicate $[SiO_4]^{4-}$, sulfate $[SO_4]^{2-}$, perchlorate $[ClO_4]^{-}$, etc. anions [8]. Therefore, the formation of the series of isostructural compounds during the synthesis of anion-mixed compounds is possible. The major requirement in this case is the electronegativity of the crystal structure and the heterovalent tetrahedral substitutions have to be compensated in the cationic part. Such substitutions are widespread in Nature and are known, in particular, for whitlockite [5,6], ardealite- [9], eulytite- [10], apatite- [11], and alunite-group minerals [12].

Sulfate $[SO_4]^{2-}$ anion plays an important role in the development of inorganic phosphors because the heterovalent $[PO_4]^{3-} \rightarrow [SO_4]^{2-}$ anion substitution is considered as the path for increasing the intensity of the luminescence [13,14]. Moreover, it has been also reported about the positive effect of the use of the mixed phosphate-sulfates for medical purposes, in particular in the restoration of bone tissue [15], and prostheses production [16,17]. As it was mentioned above, inorganic phosphors with the apatite-type structure are characterized by a large variation of substitutions in the cationic and anionic parts [18–20]. Both unsubstituted sulfates [21–23], sulfide [24] and mixed phosphate-sulfates [25,26] are known. In particular, the variety of natural sulfate-containing minerals with apatite-type structures are known and classified as members of ellestadite group with the general formula $A_{10}(SiO_4)_3(SO_4)_3X_2$, where $A = Ca^{2+}$, Pb^{2+}; $X = OH^{-}$, F^{-}, Cl^{-}. The effect of the anionic substitutions in synthetic phosphors with apatite-type structures affects the luminescent properties, due to the distortion of the coordination environment of the emission centers.

Based on the presence of natural samples with the apatite-type structures, characterized by the mixed occupancy of tetrahedral sites both by phosphate and sulfate, we could expect the similar behavior in related materials with β-$Ca_3(PO_4)_2$-type structure. In inorganic phosphors with the β-$Ca_3(PO_4)_2$-type structure the "ellestadite"-type heterovalent $[PO_4]^{3-} \rightarrow [SO_4]^{2-}$ anion substitution was performed in system $Ca_{21-x}(PO_4)_{14-2x}(SO_4)_{2x}$ ($0 < x < 1$) [27] with the limit composition $Ca_{20}(PO_4)_{12}(SO_4)_2$ at $x = 1$.

The "ellestadite"-type heterovalent $[PO_4]^{3-} \rightarrow [SO_4]^{2-}$ anion substitution in β-$Ca_3(PO_4)_2$ (Fig. 1a) structure requires coupled charge compensation with the formation of a vacancy in the crystal structure, which could be described by the following scheme (Fig. 1b):

$$[PO_4]^{3-} + ½\ Ca^{2+} = [SO_4]^{2-} + ½\ \square, \quad (1)$$

where $\square$ – is a vacancy. Based on the crystal chemistry of compounds with β-$Ca_3(PO_4)_2$-type structures, the vacancy should be located at the M4 site at three-fold axes, which is characterized by a variable occupancy a_i ($0 \leq a_i[M4] \leq 1$). The cationic sites M1–M3 and M5 are fully occupied. The vacancy could be absent, however, in this case charge compensation with the incorporation of additional monovalent ions (i.g. Li^{+}) [28] is required, and the isomorphous scheme can be written as (Fig. 1c):

$$[PO_4]^{3-} + Ca^{2+} = [SO_4]^{2-} + M^{+}. \quad (2)$$

Despite of the extensive study of inorganic materials with β-$Ca_3(PO_4)_2$-type structures, there are only few works [27,28] dedicated to the anionic substitutions of the initial host-matrix by sulfate anion. The aim of this work is the expansion of the family of materials with β-$Ca_3(PO_4)_2$-type structures *via* deeper study of the "ellestadite"-type heterovalent $[PO_4]^{3-} \rightarrow [SO_4]^{2-}$ anion substitution and determination of the influence of the $[SO_4]^{2-}$ group on the luminescent properties of the host-matrix doped with Eu^{3+} ions. To reduce the number of variable parameters in this work, we only used the scheme (1) for a clear understanding of the structure changes and their influence on the observed properties.

2. Experimental section

2.1. Materials and sample preparation

A series of mixed phosphates sulfates with the general formulas $Ca_{10.5-0.5x}(PO_4)_{7-x}(SO_4)_x$ and $Ca_{9.5-0.5x}Mg(PO_4)_{7-x}(SO_4)_x$ with $x = 0$, 0.1, and 1, have been synthesized by high-temperature solid state reaction from stoichiometric mixtures of $CaCO_3$ (99.9%), $(NH_4)_2SO_4$ (99.9%), MgO (99.9%), $CaHPO_4{\cdot}2H_2O$ (99.9%) purchased from Sigma-

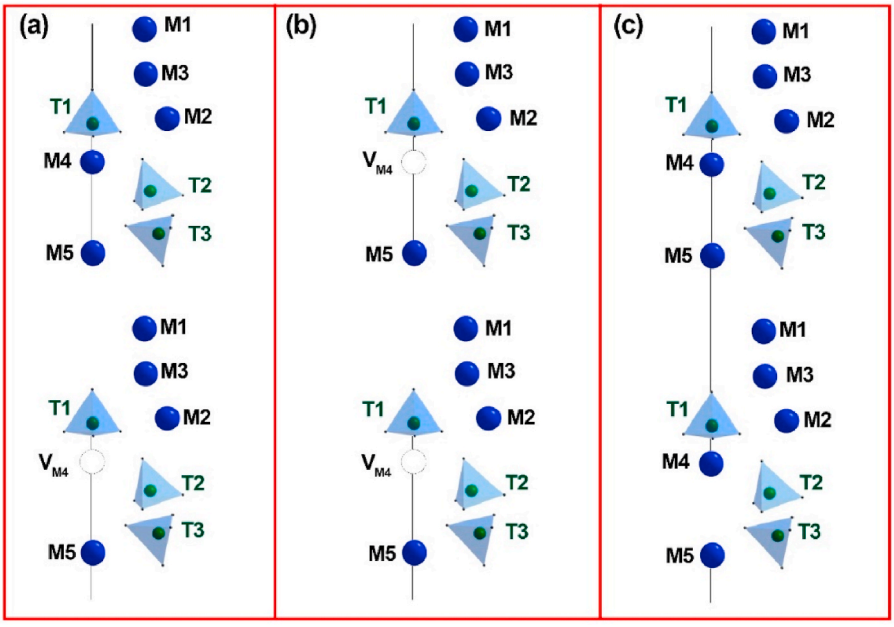

Fig. 1. The schematic representation of $[PO_4]^{3-} \rightarrow [SO_4]^{2-}$ substitution in the β-$Ca_3(PO_4)_2$-type structure: the initial β-$Ca_3(PO_4)_2$ structure (a), the substitution with coupled charge compensation with formation of vacancy in the M4 site (b), and with full occupation of the M4 site (c).

Aldrich. Another approach to synthetic road was the sol-gel method from the above starting materials. However, this synthesis leads to formation of an impurity $CaSO_4$ phase at all stages of the synthesis. Unsubstituted β-$Ca_3(PO_4)_2$ and $Ca_{9.5}Mg(PO_4)_7$ powders were synthesized as a reference.

For the study of the influence of SO_4^{2-} substitution on the luminescent properties the additional series of the Eu^{3+}-doped $Ca_9Me(PO_4)_6(SO_4)$:5%Eu^{3+} and $Ca_{9.5}Me(PO_4)_7$:5%Eu^{3+} (Me = Mg^{2+}, Zn^{2+}) were synthesized. The raw materials were $CaCO_3$ (99.9%), $(NH_4)_2SO_4$ (99.9%), MgO (99.9%), ZnO (99.9%), $CaHPO_4{\cdot}2H_2O$ (99.9%), Eu_2O_3 (99.9%) purchased from Sigma-Aldrich.

The mixtures were heated to 1273 K, and kept for 18 h with one intermediate grinding in an agate mortar, followed by slow cooling to room temperature in the furnace. Before grinding, the mixtures were slowly cooled. To prevent the formation of $CaSO_4$, $MgSO_4$, or SO_2 during heating, the mixtures were heated very slowly (during 12 h). The powder X-ray diffraction (PXRD) patterns of the prepared phases and initial reagents were checked using JCPDS PDF-4 database.

2.2. Characterization

Scanning electron microscopy (SEM) observations of $Ca_{10.5-0.5x}(PO_4)_{7-x}(SO_4)_x$ and $Ca_{9.5-0.5x}Mg(PO_4)_{7-x}(SO_4)_x$ were performed using a Tescan VEGA3 microscope equipped with an Oxford Instruments X-Max 50 silicon drift energy-dispersive X-ray spectrometry (EDXs) system with AZtec and INCA software. SEM images were acquired using secondary electron imaging and backscattered electron imaging technique. The local cation composition of disk fragments was determined by SEM-EDX.

Powder X-ray diffraction (PXRD) patterns were collected on Rigaku SmartLab SE (3 kW sealed X-ray tube, D/teX Ultra 250 silicon strip detector, vertical type θ-θ geometry, HyPix-400 (2D HPAD) detector). PXRD data were collected at room temperature in the 2θ range between 3° and 110° with a step interval of 0.02°. The LeBail decomposition was applied using JANA2006 software [29]. The crystal structure was successfully refined by the Rietveld method using RietveldToThensor [30] software. Illustrations were created with DIAMOND [31] and ATOMS [32] software.

The second harmonic generation (SHG) signal was measured with a *Q*-switched YAG:Nd laser at $\lambda_\omega = 1064$ nm in the reflection mode. The experimental set-up and arrangement have been described previously [33].

The middle infra-red (MIR) absorption spectra of the synthesized compounds were obtained on FSM 1201 FTIR spectrometer in the wavenumber region 4000–400 cm^{-1} with the spectral resolution of 2 cm^{-1} using a standard KBr disk technique.

Photoluminescence emission (PL) and excitation (PLE) spectra were measured at 300 K using a laboratory set-up based on the Lot-Oriel MS-257 spectrograph equipped with the Marconi CCD detector. A 150 W Xe arc lamp was used as an excitation source for the measurements of PL spectra, while a 40 W deuterium arc lamp – for the measurements of PLE spectra. The powder samples were placed into an optical cryostat Cryotrade LN-120. The photoluminescence spectra of all samples were obtained with spectral resolution of 0.3 nm under similar experimental conditions to compare the relative emission intensities and reduce the error. The obtained spectra were corrected for the sensitivity of the spectrometer. Gauss fit of PL spectra was performed in energy scale after the conversion of the spectra from nm scale with account of λ^2 factor.

3. Results

3.1. Powder X-ray diffraction study

The PXRD patterns of $Ca_{10.5-0.5x}(PO_4)_{7-x}(SO_4)_x$ ($x = 0.1$ and 1) obtained by solid state reaction are shown in Fig. 2. A significant amount of the impurity $CaSO_4$ phase was observed in $Ca_{10}(PO_4)_6(SO_4)$ sample

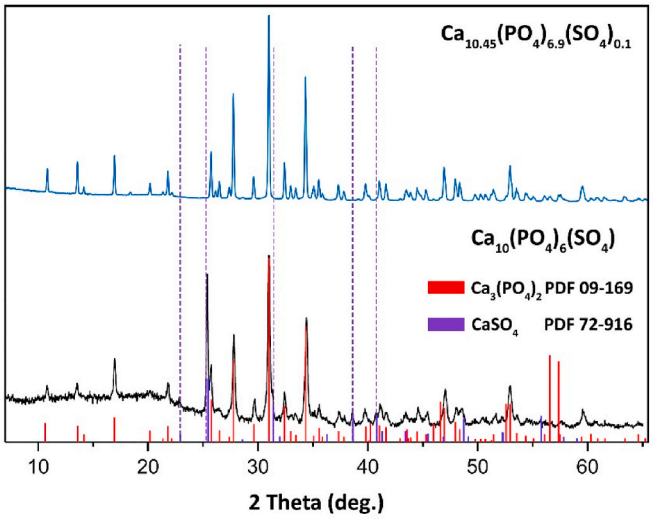

Fig. 2. PXRD patterns of $Ca_{10.45}(PO_4)_{6.9}(SO_4)_{0.1}$ and $Ca_{10}(PO_4)_6(SO_4)$ and Bragg reflections for β-$Ca_3(PO_4)_2$ (PDF2 # 09-169) and $CaSO_4$ (PDF2 # 72-916). Dotted lines show the presence of the impurity $CaSO_4$ phase in $Ca_{10}(PO_4)_6(SO_4)$.

(Fig. 2). However, the substitution for a small amount of $[SO_4]^{2-}$ avoids the formation of $CaSO_4$. Apparently, this is related to the difference in the ionic radii of S^{6+} ($r_{IV} = 0.12$ Å) and P^{5+} ($r_{IV} = 0.15$ Å), and the substitution requires the reducing of cation size in the cationic sublattice. Thus, the two-positive ions with smaller ionic radii, in comparison with Ca^{2+}, should be added for structure stabilization. Such ions can be Mg^{2+}, Zn^{2+} and Mn^{2+}, see, for instance, Refs. [34,35].

For this reason, the Mg^{2+}-doped β-$Ca_3(PO_4)_2$-type samples were synthesized, and the PXRD patterns of $Ca_{9.5-0.5x}Mg(PO_4)_{7-x}(SO_4)_x$ ($x = 0.1$ and 1) are shown in Fig. 3. No impurities of $CaSO_4$ or $MgSO_4$ phases were detected. The unit cell parameters (a, c), and volume (V) for single-phase compounds are listed in Table 1. The larger values of the unit cell parameters for $Ca_{9.45}Mg(PO_4)_{6.9}(SO_4)_{0.1}$ in comparison with $Ca_9Mg(PO_4)_6(SO_4)$ can be explained by the difference in the chemical composition of the incorporated Mg^{2+} ion (See Selection 3.2).

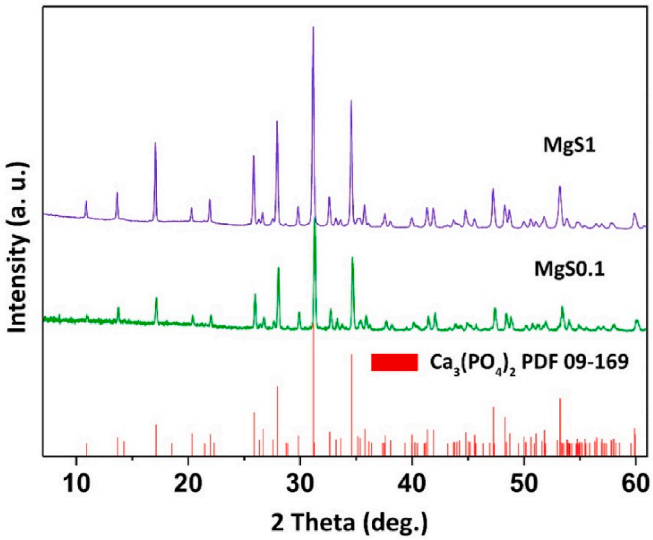

Fig. 3. PXRD patterns of $Ca_{9.5-0.5x}Mg(PO_4)_{7-x}(SO_4)_x$ ($x = 0.1$ and 1) and Bragg reflections for β-$Ca_3(PO_4)_2$ (PDF2 # 09-169).

Table 1
The unit cell parameters, SHG signal and EDX data for $Ca_{10.45}(PO_4)_{6.9}(SO_4)_{0.1}$ and $Ca_{9.5-0.5x}Mg(PO_4)_{7-x}(SO_4)_x$.

Compound	*a*, Å	*c*, Å	*V*, Å^3	SHG signal
β-$Ca_3(PO_4)_2$	10.4324(1) [36]	37.4029(1) [36]	3525.4(1) [36]	2.0
$Ca_{10.45}(PO_4)_{6.9}(SO_4)_{0.1}$	10.4284(1)	37.3889(1)	3521.36(9)	1.3
$Ca_{9.45}Mg(PO_4)_{6.9}(SO_4)_{0.1}$	10.3432(1)	37.1207(2)	3439.19(9)	0.7
$Ca_9Mg(PO_4)_6(SO_4)$	10.3618(2)	37.2361(2)	3462.32(2)	0.3

3.2. Elemental composition and SEM observations

EDX analysis of $Ca_{10.45}(PO_4)_{6.9}(SO_4)_{0.1}$ and $Ca_{9.5-0.5x}Mg(PO_4)_{7-x}(SO_4)_x$ ($x = 0.1$ and 1) were used to prove the chemical composition and presence of sulfur in the samples. The measurements were performed for 8 points of each crystallite sample. Using EDX, the Ca:P:S and Ca:Mg:P:S ratios have been obtained which were close to the expected bulk composition. The refined chemical compositions are $Ca_{9.356}Mg_{0.771}(PO_4)_{6.013}(SO_4)_{0.987}$ (CaMgS1), $Ca_{9.59}Mg_{0.86}(PO_4)_{6.9}(SO_4)_{0.1}$ (CaMgS0.1), and $Ca_{10.445}(PO_4)_{6.89}(SO_4)_{0.11}$ (CaS0.1). The SEM images of the studied samples are shown in Fig. 4. The samples with the small amount of sulfate anion form agglomerates of crystals with unregular form (Fig. 4a and b). The grain boundaries can be seen in CaMgS1 sample (Fig. 4c and d). In this sample the crystallites don't agglomerate into bulk particles. A similar morphology was observed in noncentrosymmetric β-$Ca_3(PO_4)_2$-type compounds [37]. However, the particles stick together due to preservation of noncentrosymmetric structure and slight polarization (SGH signal, Fig. 4d, Table 1). The elemental mapping of the samples shows the uniform distribution of sulfur in the samples (Fig. 4e).

3.3. Fourier-transform infrared spectroscopy

Fourier-transform infrared spectroscopy was used to confirm the presence of SO_4 group in the crystal structure. The FT-IR spectra of synthesized compounds are shown in Fig. 5. The slight difference between sulfur and phosphorus atomic masses and also P – O and S – O distances in tetrahedral coordination predetermine the difficulties with P – O and S – O vibrations separation [38–40]. However, the difference in the charge of S^{6+} in comparison with P^{5+} causes a slight shift of internal SO_4 vibrations to higher wavenumbers. The fundamental frequencies of SO_4 unit internal vibrations (ν_1 – 983 cm^{-1}, ν_2 – 450 cm^{-1}, ν_3 – 1105 cm^{-1}, ν_4 – 611 cm^{-1}) are slightly higher than the vibrations of PO_4 unit (ν_1 – 938 cm^{-1}, ν_2 – 420 cm^{-1}, ν_3 – 1017 cm^{-1}, ν_4 – 567 cm^{-1}) [41].

The absorption bands in the region 1250-500 cm^{-1} are due to internal vibrations of phosphate and sulfate tetrahedra. The theoretical group analysis for similar compounds $Ca_{9-x}Zn_xLa(PO_4)_7$ with the same space group *R*3*c* was performed in Ref. [37]. In $Ca_3(PO_4)_2$ spectrum (Fig. 5a) the absorption bands at 1220 – 1000 cm^{-1} were assigned to antisymmetrical stretching ν_3 vibrations and symmetrical stretching ν_1 vibrations, which reveal as two bands at 971 and 945 cm^{-1}. The bands of antisymmetrical bending vibrations ν_4 are observed at 650 – 500 cm^{-1} as a typical doublet of bands at 606 and 553 cm^{-1} with several shoulders. The spectrum of $Ca_{10.45}(PO_4)_{6.9}(SO_4)_{0.1}$ (Fig. 5b) is almost identical to the spectrum of pure phosphate (Fig. 5a). The changes that we can trace in spectrum at Fig. 5c belonging to $Ca_{9.45}Mg(PO_4)_{6.9}(SO_4)_{0.1}$ compound are caused by the distortion of anionic tetrahedral groups (PO_4, SO_4) due to the isomorphic Ca →Mg substitution in M5 sites. The significant change of spectral pattern due to substitutions in the anionic part of the crystal structure can be observed at the spectrum of $Ca_9Mg(PO_4)_6(SO_4)$ (Fig. 5d). The wide absorption band at 1091 cm^{-1}, which is typical for antisymmetrical stretching vibrations of SO_4^{2-} tetrahedral ion [42–44] appears in $Ca_9Mg(PO_4)_6(SO_4)$ in comparison to pure phosphate spectrum. In the region of bending vibrations, the occurrence of a new low

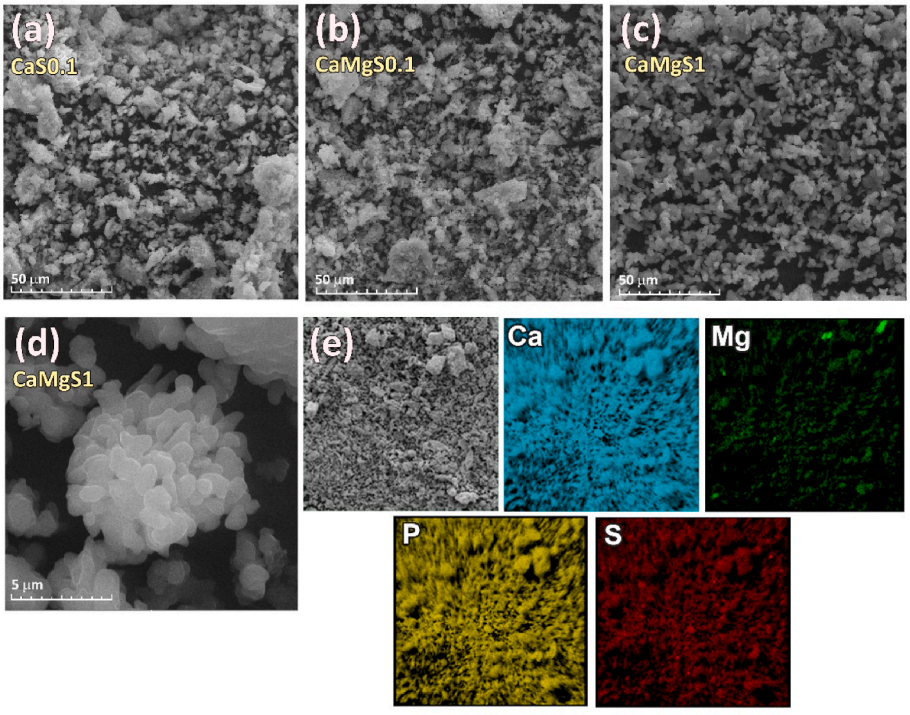

Fig. 4. The SEM images of $Ca_{10.45}(PO_4)_{6.9}(SO_4)_{0.1}$ (a), $Ca_{9.45}Mg(PO_4)_{6.9}(SO_4)_{0.1}$ (b) and $Ca_9Mg(PO_4)_6(SO_4)$ (c). The enlarged SEM image of a particle (d) and elemental mapping (e) of $Ca_9Mg(PO_4)_6(SO_4)$.

intensity band at 635 cm^{-1} is also evidence of SO_4 group presence. The diffuse and illegible character of the corresponding spectrum indicate statistically disordered isomorphic substitutions in anionic tetrahedra. The absence of absorption bands in the region 4000 – 1300 cm^{-1} indicate the absence of O – H bonds in the crystal structure.

3.4. SHG study

An additional confirmation that the $[SO_4]^{2-}$ group was successfully introduced into the β-$Ca_3(PO_4)_2$-type structure is the SHG study (Table 1). SHG measurements can be useful for the determination of the presence/absence of the symmetry center in the lattice cell. Previously, it was shown [45] that β-$Ca_3(PO_4)_2$-type compounds are characterized by polar (space group *R*3*c*) [46] and non-polar [space groups $R\bar{3}c$ [47] and $R\bar{3}m$ [48] (high-temperature phase)] structures. The presence of even a weak SHG signal response ($I_{2\omega}/I_{2\omega}(SiO_2)$) is evidence of polar structure.

The incorporation of $[SO_4]^{2-}$ in the unit cell with charge compensation requires the formation of a vacancy in the M4 site (Fig. 1). A small $[PO_4]^{3-} \rightarrow [SO_4]^{2-}$ substitution in $Ca_{10.45}(PO_4)_{6.9}(SO_4)_{0.1}$ leads to an approximately half-occupied M4 site (a_i[M4] = 0.445) (Table S1 of the Supporting Information). This value differs a little from pure phosphate β-$Ca_3(PO_4)_2$ (a_i[M4] = 0.5) [36], and this is the reason for a slight difference in the SHG signal of CaS0.1 ($I_{2\omega}/I_{2\omega}(SiO_2) \sim 1.3$ in comparison with pure β-$Ca_3(PO_4)_2$ ($I_{2\omega}/I_{2\omega}(SiO_2)$ [β-$Ca_3(PO_4)_2$] ~ 2. In $Ca_9Mg(PO_4)_6(SO_4)$ the occupation of the M4 site decreases (a_i[M4] = 0.127, Table S2 of the Supporting Information) (Fig. 1), and the SHG signal drops (Table 1). However, its presence confirms structure refinement in the polar space group (*R*3*c*) for all samples.

3.5. Crystal structure refinement

According to SHG measurements, structure refinement was performed in the *R*3*c* space group for CaS0.1, CaMgS0.1, and CaMgS1 samples. Thus, the crystal structures of solid solutions were refined starting from the positional parameters of $Ca_{19}Mg_2(PO_4)_{14}$ [49]. The background was described by a Chebyshev polynomial function (31st order). Pseudo-Voigt functions were used for fitting the reflection profiles. Among structural parameters, we refined the atomic coordinates and the isotropic temperature factor, which were constrained to be the same for all atoms. The free refinement of calcium positions showed partial occupancy of Ca4 positions (~0.44, 0.48, and 0.22 for CaS0.1, MgS0.1 and MgS1, respectively). Then, the Ca and Mg atoms were disordered over M5 sites and their occupancies were refined with total occupancy restrained to unity resulting in ~0.87, 0.73 of magnesium occupancies for MgS0.1 and MgS1 samples, respectively. So, occupancy refinement is in good agreement with the EDX data and the formulas were fixed accordingly ($Ca_{10.5-0.5x-y}Mg_y(PO_4)_{7-x}(SO_4)_x$: $x = 0.1$, $y = 0.86$ (MgS0.1); $x = 0.11$, $y = 0$ (CaS0.1); $x = 0.987$, $y = 0.771$ (MgS1)). We determined the occupation factor of the Ca4 site as y–x while the occupation factors of the magnesium and calcium atoms in the M5 were taken as y and 1–y, respectively. The sulfur and phosphorus atoms were disordered over T2 sites and their occupancies were taken as $x/3$ and 1–$x/3$, respectively. Main crystallographic data and experimental details of $Ca_{10.5-0.5x-y}Mg_y(PO_4)_{7-x}(SO_4)_x$, $x = 0.1$, $y = 0.86$; $x = 0.11$, $y = 0$; $x = 0.987$, $y = 0.771$ are listed in Table 2. Tables S1–S3 of the Supporting Information contain atomic coordinates, displacement parameters and site-occupancy factors, and Tables S4 and S5 include selected bond distances and angles, respectively. CCDC 2142920, 2142921, 2142922 contain the supplementary crystallographic data for this paper. The final results of the refinement are presented in Fig. S1 of the Supporting Information.

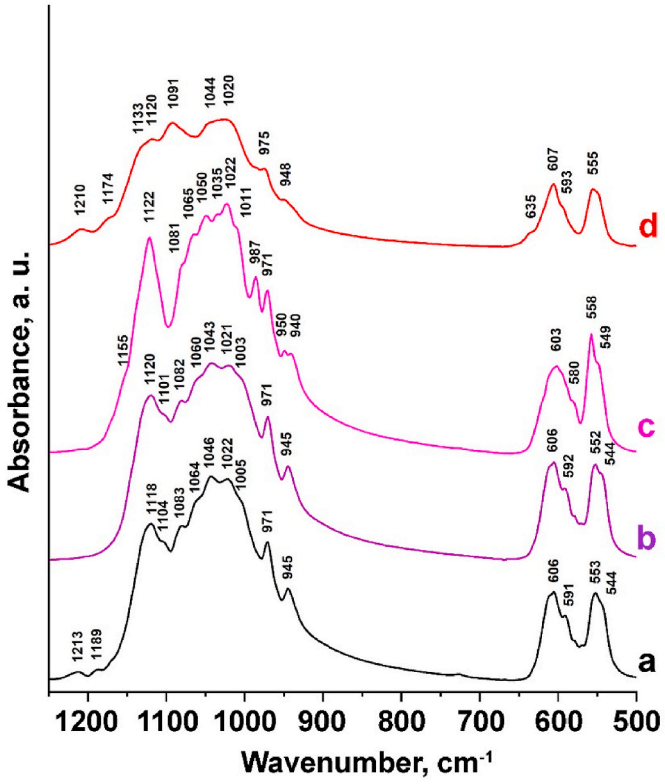

Fig. 5. FT-IR spectra of β-$Ca_3(PO_4)_2$ (a), $Ca_{10.45}(PO_4)_{6.9}(SO_4)_{0.1}$ (b), $Ca_{9.45}Mg(PO_4)_{6.9}(SO_4)_{0.1}$ (c), $Ca_9Mg(PO_4)_6(SO_4)$ (d).

3.6. Photoluminescence properties

The photoluminescence properties were studied for $Ca_9Me(PO_4)_6(SO_4)$:5%Eu^{3+} and $Ca_{9.5}Me(PO_4)_7$:5%Eu^{3+} as a reference, where Me = Mg^{2+}, Zn^{2+}. The PLE spectra of studied samples are presented in Fig. 6. The spectra consist of a set of narrow lines in the range 290–470 nm originating from intracenter 4f–4f transitions within Eu^{3+} ions and a broad band observed in the region of 200–290 nm, which arise due to charge transfer transitions from 2pO to 4fEu states. The PLE profile is same for the samples containing Mg^{2+} [46] and Zn^{2+} [45,50] cations, however, the introduction of $[SO_4]^{2-}$ groups results in the slight shift of the CTB maximum from 244 to 247 nm (Fig. 6, dotted line) and broadening of the CTB. The energy of charge transfer transitions depends on the Eu–O bond length, which varies with the introduction of $[SO_4]^{2-}$ groups into the sample's composition.

The PL spectra are presented in Fig. 7. The spectra consist of a group of intense lines in the region 580 – 720 nm, which arise due to $^5D_0 \rightarrow {}^7F_J$ (J = 0–4) transitions and a group of less intensive lines in the region 520–570 nm, which arise due to transitions from upper excited term $^5D_1$ to $^7F_{1,2}$ terms of Eu^{3+} (Fig. 7, inset (a)).

The integrated intensities of Eu^{3+} emission are presented in Fig. 7, inset (b). As it follows from the figure, the introduction of $[SO_4]^{2-}$ groups resulted in the 65% reduction of Eu^{3+} emission intensity for both series of samples with Mg^{2+} and Zn^{2+} ions. The most intensive emission was observed for the $Ca_{9.5}Zn(PO_4)_7$:5%Eu^{3+} sample. The positive influence of structure modification on luminescent properties by Zn^{2+} instead of other ions was previously established in other β-$Ca_3(PO_4)_2$-based phosphors [37,51]. The main reason for such an improvement is based on increased polyhedra distortion [47] and the influence of first and second coordination spheres of Eu^{3+} environment [52].

To estimate the contribution of the SO_4^{2-} anion to the luminescent properties the polyhedra distortion index (DI) was calculated for the synthesized samples along with the undoped compounds using the following equitation [46]:

Table 2
Main Crystallographic Data and experimental details for $Ca_{10.5-0.5x-y}Mg_y(PO_4)_{7-x}(SO_4)_x$, $x = 0.1$, $y = 0.86$; $x = 0.11$, $y = 0$; $x = 0.987$, $y = 0.771$.

Phase	$Ca_{9.59}Mg_{0.86}(PO_4)_{6.9}(SO_4)_{0.1}$	$Ca_{10.445}(PO_4)_{6.89}(SO_4)_{0.11}$	$Ca_{9.356}Mg_{0.771}(PO_4)_{6.013}(SO_4)_{0.987}$
Abbreviation	CaMgS0.1	CaS0.1	CaMgS1
M_r	1070.17	1083.52	1059.3
Temperature, °C	300		
Crystal system, Space Group	Trigonal, *R3c*		
a, *c* (Å)	10.3432(1), 37.1207(2)	10.4284(1), 37.3889(1)	10.3618(2), 37.2361(2)
V (Å^3)	3439.19(9)	3521.36(9)	3462.32(2)
Z	6		
D_x (Mg m^{-3})	3.1002	3.0657	3.0484
Radiation type	Cu *Kα*		
Diffractometer	Rigaku SmartLab SE		
θ-Range	3–110, step size (°) 0.02		
R_{wp}	0.055	0.048	0.059
R_p	0.058	0.031	0.060
R_{Bragg}	0.045	0.033	0.048
S	1.39	2.04	2.51
No. of parameters	83	80	82

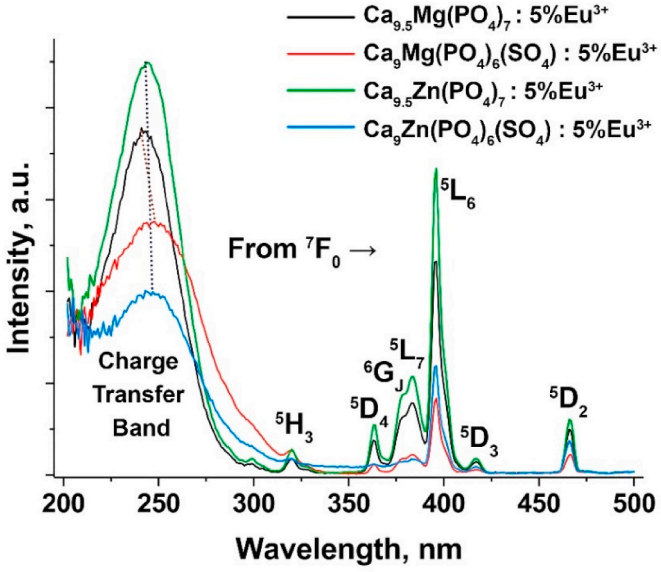

Fig. 6. PLE spectra of $Ca_9Me(PO_4)_6(SO_4)$:5%Eu^{3+} and $Ca_{9.5}Me(PO_4)_7$:5%Eu^{3+} (Me = Mg^{2+}, Zn^{2+}) at λ_{em} = 615 nm, T = 300 K.

$$DI = \frac{1}{n}\sum_{i=1}^{n}\frac{|l_i - l_{av}|}{l_{av}}$$

where *n* is the coordination number of the central cation, l_i is the distance from the central cation to the O atom, and l_{av} is the average bond length for the selected polyhedra. DI was calculated for each of M1–M3 polyhedra, which can be occupied by Eu^{3+}. The data are given in Table S6 and Fig. 8. The distortion of polyhedra is the highest and the symmetry of the averaged crystal field of the ligands is the lowest for $Ca_{9.5}Zn(PO_4)_7$ (ICDD No 04-020-2028) (Fig. 8). These data explain the higher intensity of luminescence for Zn^{2+} containing $Ca_{9.5}Zn(PO_4)_7$:5% Eu^{3+} and $Ca_9Zn(PO_4)_6(SO_4)$:5%Eu^{3+} samples. As the result, the samples with $[PO_4]^{3-} \rightarrow [SO_4]^{2-}$ substitution ($Ca_9Zn(PO_4)_6(SO_4)$:5%Eu^{3+} and $Ca_9Mg(PO_4)_6(SO_4)$:5%Eu^{3+}) show a lower intensity of luminescence than unsubstituted phosphates ($Ca_{9.5}Zn(PO_4)_7$:5%Eu^{3+} and $Ca_{9.5}Mg(PO_4)_7$:5%Eu^{3+}). However, the SHG signals for studied compounds are almost the same (Table 3).

The small $PO_4^{3-} \rightarrow SO_4^{2-}$ substitution in CaS0.1 has little effect on DI in comparison with β-$Ca_3(PO_4)_2$. Perhaps, the reason for a positive effect of SO_4^{2-} substitution in $Ca_{3-x}Li_x(PO_4)_{2-x}(SO_4)_x$:2%$Dy^{3+}$ [28] was related to Li^+ ions in the β-$Ca_3(PO_4)_2$-type structure. Such regularities with the introduction of lithium into whitlockite-type hosts were previously

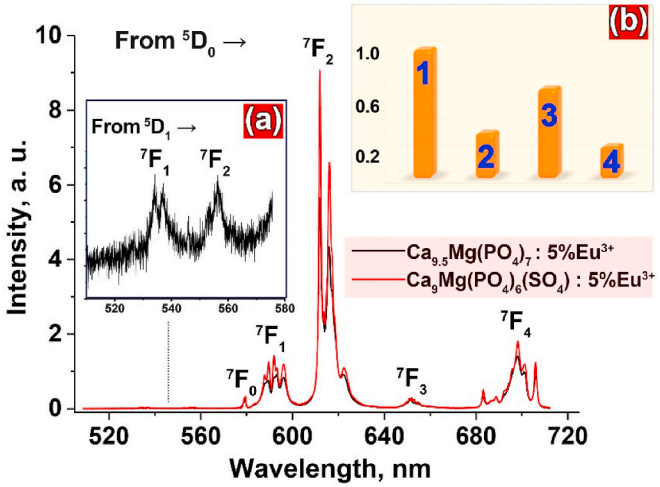

Fig. 7. PL spectra of $Ca_{9.5-0.5x}Mg(PO_4)_{7-x}(SO_4)_x$:5%$Eu^{3+}$ (x = 0 and 1) at λ_{exc} = 396 nm, T = 300 K. The inset (a) shows the enlarged transitions from $^5D_1$ state. The inset (b) shows the relative emission intensity of $Ca_{9.5}Zn(PO_4)_7$:5% Eu^{3+} (1), $Ca_9Zn(PO_4)_6(SO_4)$:5%Eu^{3+} (2), $Ca_{9.5}Mg(PO_4)_7$:5%Eu^{3+} (3), $Ca_9Mg(PO_4)_6(SO_4)$:5%Eu^{3+} (4); PL spectra was integrated in the spectral region 520–710 nm.

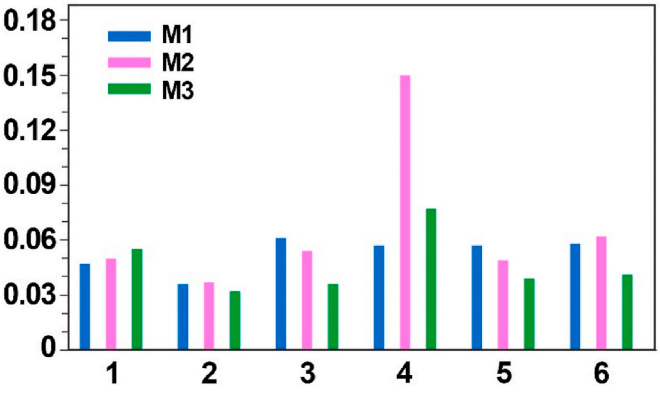

Fig. 8. Calculated polyhedra disortion index DI for M1–M3 polyhedra in $Ca_{9.356}Mg_{0.771}(PO_4)_{6.013}(SO_4)_{0.987}$ (1), $Ca_{2.71}Mg_{0.29}(PO_4)_2$ (2), $Ca_{9.59}Mg_{0.86}(PO_4)_{6.9}(SO_4)_{0.1}$ (3), $Ca_{9.5}Zn(PO_4)_7$ (4), β-$Ca_3(PO_4)_2$ (5), $Ca_{10.445}(PO_4)_{6.89}(SO_4)_{0.11}$ (6).

Table 3
SHG signals and lifetimes for $Ca_9Me(PO_4)_6(SO_4)$:5%Eu^{3+} and $Ca_{9.5}Me(PO_4)_7$:5%Eu^{3+} (Me = Mg^{2+}, Zn^{2+}).

	SHG signal	τ, μs
$Ca_{9.5}Mg(PO_4)_7$:5%Eu^{3+}	2.1	1.834
$Ca_9Mg(PO_4)_6(SO_4)$:5%Eu^{3+}	0.3	1.876
$Ca_{9.5}Zn(PO_4)_7$:5%Eu^{3+}	2.0	1.843
$Ca_9Zn(PO_4)_6(SO_4)$:5%Eu^{3+}	0.3	1.877

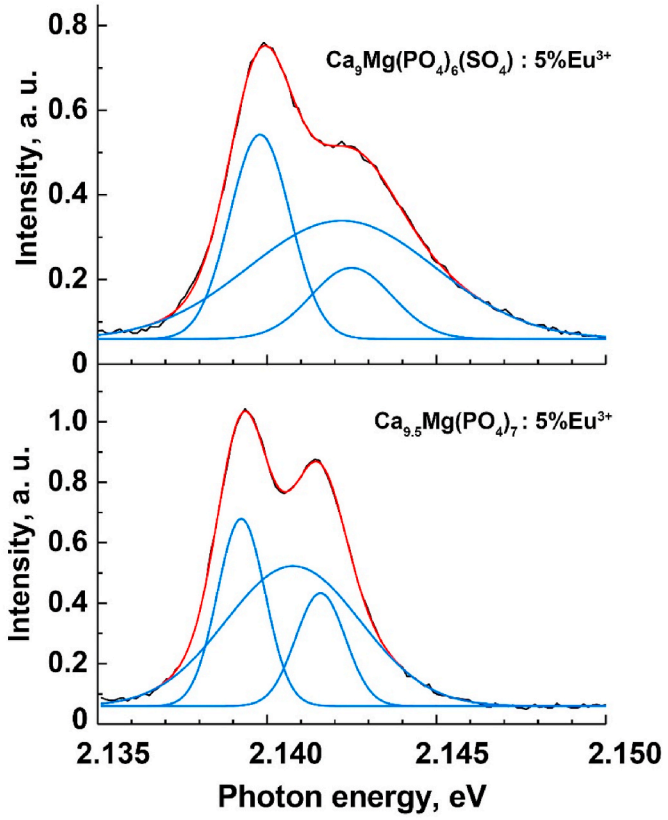

Fig. 9. PL spectra in the region of $^5D_0 \rightarrow {}^7F_0$ transitions of $Ca_9Mg(PO_4)_6(SO_4)$:5%Eu^{3+} and $Ca_{9.5}Mg(PO_4)_7$:5%Eu^{3+} and their decomposition on Gaussian curves.

observed in Refs. [53,54].

The details of emission spectra in the region of $^5D_0 \rightarrow {}^7F_0$ transitions are presented in Fig. 9 for samples with Mg^{2+} cation. The corresponding transition is forbidden and can be observed when Eu^{3+} occupies the non-centrosymmetric site in the crystal lattice. Two pronounced peaks were observed for $Ca_{9.5}Mg(PO_4)_7$:5%Eu^{3+}. However, three Gaussian curves are needed for the reliable fit of the emission spectra, thus indicating that Eu^{3+} ions occupy three non-equivalent sites in the crystal lattice. The introduction of $[SO_4]$ groups results in a slight shift of the peaks to the high energy region. The position of $^5D_0 \rightarrow {}^7F_0$ bands depends on the Eu–O bond length due to the nephelauxetic effect [55,56] and shifts toward higher energies when the distance between Eu and O increases. Moreover, the profile of the $^5D_0 \rightarrow {}^7F_0$ peak broadens and the Gaussian curves broadens as well. The broadening is associated with the partial structural disorder and redistribution of the mean distances' values (Table S6) in M1–M3 polyhedral, which arise due to the substitution of PO_4 tetrahedra by SO_4 ones.

The measured lifetimes are listed in Table 3. With a general decrease in luminescence efficiency in sulfur-containing samples, lifetimes tend to increase. The higher local distortion of the Eu^{3+} environment in the phosphates results in shorter luminescence lifetimes in comparison with sulfur-substituted samples according to higher probability of the radiative transitions.

4. Conclusions

In this paper we propose a new route to design inorganic phosphors with β-$Ca_3(PO_4)_2$-type structure via the "ellestadite"-type heterovalent $[PO_4]^{3-} \rightarrow [SO_4]^{2-}$ anionic substitution. This new route significantly expands the crystal chemistry of materials with β-$Ca_3(PO_4)_2$-type structures and gives more insights into the deeper understanding of the dependence of luminescent properties on the cation distribution. It was found that $[PO_4]^{3-} \rightarrow [SO_4]^{2-}$ substitution requires the reducing of cation size in the cationic sublattice or can be realized in a small range in the initial β-$Ca_3(PO_4)_2$ phosphate. The reducing of the cationic sublattice was performed through the incorporation of Mg^{2+} and Zn^{2+} ions. The polar structure was confirmed for all synthesized samples by the presence of SHG response. According to the PXRD study, the preferred site in the anionic sublattice is T2, and this assumption was based on the interatomic distances analysis. The photoluminescent properties study of the $[SO_4]^{2-}$ substituted phosphates shows that the Zn^{2+} containing samples exhibit a 1.5 times higher intensity in comparison with the Mg^{2+} containing samples. Such dependence was also observed in other substituted phosphates and explained to be due to the higher rate of polyhedra distortion in the Zn^{2+} containing samples. The absence of positive effect of the heterovalent $[PO_4]^{3-} \rightarrow [SO_4]^{2-}$ substitution in β-$Ca_3(PO_4)_2$-host matrix doped by Eu^{3+} on the luminescent properties, in comparison with $Ca_{3-x}Li_x(PO_4)_{2-x}(SO_4)_x$:2%$Dy^{3+}$ [28] can be probably explained by (i) the presence of Li^+ ions in the β-$Ca_3(PO_4)_2$-type structure and (ii) the difference between crystal chemical features of Dy^{3+} and Eu^{3+} ions. The obtained results allow to enrich the crystal chemistry of substituted and co-substituted phosphates.

Declaration of competing interest

The authors declare that they have no known competing financial interests or personal relationships that could have appeared to influence the work reported in this paper.

Acknowledgments

D.V.D. is grateful to the Scholarship of the President of the Russia Federation (СП-859.2021.1). D.A.S. is grateful for financial support of the Estonian Research Council, project PUT PRG111. The study was supported by the Development Program of the Interdisciplinary Scientific and Educational School of Lomonosov Moscow State University's "The future of the planet and global environmental change" and the state assignment of the Chemistry Department of Moscow State University (Agreement No. AAAA-A21-121011590086-0). The X-ray study was carried out in accordance with the state of the Russian Federation, state registration number 122011300125-2.

Appendix A. Supplementary data

Supplementary data to this article can be found online at https://doi.org/10.1016/j.ceramint.2022.05.077.

References

[1] T.J. White, D. ZhiLi, Structural derivation and crystal chemistry of apatites, Acta Crystallogr. Sect. B Struct. Sci. 59 (2003) 1–16, https://doi.org/10.1107/S0108768102019894.

[2] H.-K. Liu, L.-B. Liao, Y.-Y. Zhang, S.M. Aksenov, N. Liu, Q.-F. Guo, D.V. Deyneko, T.-Y. Wang, L.-F. Mei, C.-H. Sun, Computational analysis of apatite-type compounds for band gap engineering: DFT calculations and structure prediction using tetrahedral substitution, Rare Met. 40 (2021) 3694–3700, https://doi.org/10.1007/s12598-020-01690-0.

[3] H. Liu, L. Liao, S.M. Aksenov, Q. Guo, L. Mei, D.V. Deyneko, Novel Dy^{3+}-doped Ge^{4+}-substituted apatite-type phosphors, $Ca_9La(PO_4)_5[(Si_{1-x}Ge_xO_4)]F_2$:$Dy^{3+}$:

synthesis, structure, crystal chemical features, and luminescent properties, Ceram. Int. 47 (2021) 23300–23308, https://doi.org/10.1016/j.ceramint.2021.05.043.

[4] H. Liu, Y. Zhang, L. Mei, Q. Guo, H. Li, L. Liao, Tetrahedral substitution to induce tunable luminescent properties in apatite structural solid-solution phosphors $Ca_9La(PO_4)_5[(Si,Ge)O_4]F_2$:Ce^{3+}, Dyes Pigments 145 (2017) 514–517, https://doi.org/10.1016/j.dyepig.2017.06.045.

[5] V.V. Titkov, E.V. Latipov, O.V. Baryshnikova, B.I. Lazoryak, F.D. Fedyunin, D. A. Spassky, P.B. Dzhevakov, D.V. Deyneko, Influence of anionic substitutions on the luminescent properties of $Ca_{9.75}Eu_{0.5}(VO_4)_7$, J. Solid State Chem. 308 (2022), 122884, https://doi.org/10.1016/j.jssc.2022.122884.

[6] D.V. Deyneko, I.V. Nikiforov, B.I. Lazoryak, S.M. Aksenov, The role of anionic heterovalent $[PO_4]^{3-} \rightarrow [GeO_4]^{4-}$ substitution on the luminescence properties of inorganic phosphors with the β-$Ca_3(PO_4)_2$-type structure: new data based on accurate crystal structure refinement, Dalton Trans. 51 (2022) 655–663, https://doi.org/10.1039/D1DT03534G.

[7] V.V. Titkov, S.Y. Stefanovich, D.V. Deyneko, Y.Y. Dikhtyar, S.M. Aksenov, O. V. Baryshnikova, A.A. Belik, B.I. Lazoryak, Isovalent and aliovalent cation substitutions in the anion sublattice of whitlockite-type ferroelectrics $Ca_9RE(VO_4)_7$ with RE =Y and Yb, J. Solid State Chem. 279 (2019), 120966, https://doi.org/10.1016/j.jssc.2019.120966.

[8] D.E.C. Corbridge, Phosphorus, CRC Press, 2016, https://doi.org/10.1201/b12961.

[9] R.V. Gaines, H.C.W. Skinner, E.E. Foord, B. Mason, A. Rosenzweig, DANA'S NEW MINERALOGY, eighth ed., John Wiley & Sons, Inc., New York, 1997.

[10] V.I. Pet'kov, A.S. Dmitrienko, A.I. Bokov, Thermal expansion of phosphate–sulfates of eulytite structure, J. Therm. Anal. Calorim. 133 (2018) 199–205, https://doi.org/10.1007/s10973-017-6676-7.

[11] C.M. Mehare, Y.R. Parauha, V. Chopra, S. Ray, N.S. Dhoble, C. Ghanty, S.J. Dhoble, Tailoring the luminescent properties of $Ca_9La(PO_4)_5(SiO_4)F_2$:1 mol%Eu^{3+} phosphor via doping of chloride, molybdate, vanadate, sulfate, and tungstate ions, J. Mater. Sci. Mater. Electron. 31 (2020) 3426–3440, https://doi.org/10.1007/s10854-020-02891-0.

[12] N.D. Owen, N.J. Cook, R. Ram, B. Etschmann, K. Ehrig, D.S. Schmandt, M. Rollog, P. Guagliardo, J. Brugger, The dynamic uptake of lead and its radionuclides by natural and synthetic aluminium-phosphate-sulfates, Miner. Eng. 160 (2021), 106659, https://doi.org/10.1016/j.mineng.2020.106659.

[13] Q. Guo, B. Ma, L. Liao, M.S. Molokeev, L. Mei, H. Liu, Crystal structure and luminescence properties of novel $Sr_{10-x}(SiO_4)_3(SO_4)_3O$:$xEu^{2+}$ phosphor with apatite structure, Ceram. Int. 42 (2016) 11687–11691, https://doi.org/10.1016/j.ceramint.2016.04.086.

[14] F. Nouri, G. Panczer, Y. Guyot, M. Trabelsi-Ayadi, R. Ternane, Synthesis and luminescent properties of Eu^{3+}-doped phosphate-sulfate fluorapatites $Ca_{10-x}Na_x(PO_4)_{6-x}(SO_4)_xF_2$, J. Lumin. 192 (2017) 590–594, https://doi.org/10.1016/j.jlumin.2017.07.033.

[15] K. Cheng, W. Zhu, X. Weng, L. Zhang, Y. Liu, C. Han, W. Xia, Injectable tricalcium phosphate/calcium sulfate granule enhances bone repair by reversible setting reaction, Biochem. Biophys. Res. Commun. 557 (2021) 151–158, https://doi.org/10.1016/j.bbrc.2021.03.145.

[16] M. Jarcho, R.L. Salsbury, M.B. Thomas, R.H. Doremus, Synthesis and fabrication of β-tricalcium phosphate (whitlockite) ceramics for potential prosthetic applications, J. Mater. Sci. 14 (1979) 142–150, https://doi.org/10.1007/BF01028337.

[17] Z. Cai, Z. Wu, Y. Wan, T. Yu, C. Zhou, Manipulation of the degradation behavior of calcium phosphate and calcium sulfate bone cement system by the addition of micro-nano calcium phosphate, Ceram. Int. 47 (2021) 29213–29224, https://doi.org/10.1016/j.ceramint.2021.07.086.

[18] V. Paterlini, M. Bettinelli, R. Rizzi, A. El Khouri, M. Rossi, G. Della Ventura, F. Capitelli, Characterization and luminescence of Eu^{3+}- and Gd^{3+}-doped hydroxyapatite $Ca_{10}(PO_4)_6(OH)_2$, Crystals 10 (2020) 806, https://doi.org/10.3390/cryst10090806.

[19] G.A. Waychunas, Apatite luminescence, Rev. Mineral. Geochem. 48 (2002) 701–742, https://doi.org/10.2138/rmg.2002.48.19.

[20] M. Gaft, R. Reisfeld, G. Panczer, Modern Luminescence Spectroscopy of Minerals and Materials, Springer International Publishing, Cham, 2015, https://doi.org/10.1007/978-3-319-24765-6.

[21] A. Piotrowski, V. Kahlenberg, R. Fischer, The solid solution series of the sulfate apatite system $Na_{6.45}Ca_{3.55}(SO_4)_6(F_xCl_{1-x})_{1.55}$, J. Solid State Chem. 163 (2002) 398–405, https://doi.org/10.1006/jssc.2001.9408.

[22] F. Yang, L. Wang, Y. Ge, L. Huang, D. Gao, J. Bi, G. Zou, $K_4Sb(SO_4)_3Cl$: the first apatite-type sulfate ultraviolet nonlinear optical material with sharply enlarged birefringence, J. Alloys Compd. 834 (2020), 155154, https://doi.org/10.1016/j.jallcom.2020.155154.

[23] P.S. Thakre, S.C. Gedam, S.J. Dhoble, R.G. Atram, Luminescence investigations on sulfate apatite $Na_6(SO_4)_2FCl$:RE (RE = Dy, Ce or Eu) phosphors, J. Lumin. 131 (2011) 2683–2689, https://doi.org/10.1016/j.jlumin.2011.06.050.

[24] C. Liang, H. You, Y. Fu, X. Teng, K. Liu, J. He, Luminescence properties of a tunable blue-green-emitting $Ca_{10}(PO_4)_6S$:Ce^{3+},Tb^{3+} phosphors for UV-excited white LEDs, Optik (Stuttg) 131 (2017) 335–342, https://doi.org/10.1016/j.ijleo.2016.11.099.

[25] N. Faten, R. Ternane, Ayadi Malika, Synthesis and ionic conductivity of PhosphateSulfate fluorapatites $Ca_{10-x}Na_x(PO_4)_{6-x}(SO_4)_xF_2$ (x = 0;3;6), 2021.

[26] F. Nouri, G. Panczer, M. Trabelsi-ayadi, R. Ternane, Synthesis and vibrational study of phosphate-sulfate fluorapatites academic discipline and sub-disciplines, J. Luminescence 12 (2016) 4975–4980.

[27] M. Marraha, J.C. Heughebaert, Preparation et Etude Physico-Chimique d'une Serie de Phosphosulfates de Calcium $Ca_{21-x}(PO_4)_{14-2x}(SO_4)_{2x}$ (Formula Omitted) Presentant La Structure de l'orthophosphate Tricalcique Anhydre β-$Ca_3(PO_4)_2$, Phosphorus. Sulfur, Silicon Relat. Elem. 44 (1989) 177–192, https://doi.org/10.1080/10426508908040607.

[28] M. Yu, X. Xu, W. Zhang, X. Chen, P. Zhang, Y. Huang, The effect of Sm^{3+} co-doping on the luminescence properties of $Ca_{2.85}Li_{0.15}(PO_4)_{1.85}(SO_4)_{0.15}$:$Dy^{3+}$ white-emitting phosphors, J. Alloys Compd. 817 (2020) 1–9, https://doi.org/10.1016/j.jallcom.2019.152761.

[29] V. Petricek, M. Dusek, L. Palatinus, V. Petrícek, M. Dušek, L. Palatinus, Crystallographic computing system JANA2006: general features, Zeitschrift Krist. 229 (2014) 345–352, https://doi.org/10.1515/zkri-2014-1737.

[30] R.S. Bubnova, V.A. Firsova, S.N. Volkov, S.K. Filatov, RietveldToTensor: Program for processing powder X-ray diffraction data under variable conditions, Glas. Phys. Chem. 44 (2018) 33–40, https://doi.org/10.1134/S1087659618010054.

[31] K. Brandenburg, DIAMOND, Version 2.1c, Crystal Impact 627 GbR, Bonn, Germany, 1999 (n.d.).

[32] E. Dowty, ATOMS. Version 6.1. Shape Software, Kingsport, TN 37663, USA, 2003. http://www.shapesoftware.com.

[33] D.V. Deyneko, V.A. Morozov, J. Hadermann, A.E. Savon, D.A. Spassky, S. Y. Stefanovich, A.A. Belik, B.I. Lazoryak, A novel red $Ca_{8.5}Pb_{0.5}Eu(PO_4)_7$ phosphor for light emitting diodes application, J. Alloys Compd. 647 (2015) 965–972, https://doi.org/10.1016/j.jallcom.2015.06.123.

[34] R. Sasidharan Pillai, V.M. Sglavo, Effect of MgO addition on solid state synthesis and thermal behavior of beta-tricalcium phosphate, Ceram. Int. 41 (2015) 2512–2518, https://doi.org/10.1016/j.ceramint.2014.10.073.

[35] X. Wei, M. Akinc, Crystal structure analysis of Si- and Zn-codoped tricalcium phosphate by neutron powder diffraction, J. Am. Ceram. Soc. 90 (2007) 2709–2715, https://doi.org/10.1111/j.1551-2916.2007.01764.x.

[36] M. Yashima, A. Sakai, T. Kamiyama, A. Hoshikawa, Crystal structure analysis of β-tricalcium phosphate $Ca_3(PO_4)_2$ by neutron powder diffraction, J. Solid State Chem. 175 (2003) 272–277, https://doi.org/10.1016/S0022-4596(03)00279-2.

[37] Y.Y. Dikhtyar, D.V. Deyneko, K.N. Boldyrev, E.Y. Borovikova, A.S. Lipatiev, S. Y. Stefanovich, B.I. Lazoryak, Luminescent properties of Er^{3+} in centrosymmetric and acentric phosphates $Ca_8MEr(PO_4)_7$ (M = Ca, Mg, Zn) and $Ca_{9-x}Zn_xLa(PO_4)_7$:Er^{3+}, Mater. Res. Bull. 138 (2021), 111244 https://doi.org/10.1016/j.materresbull.2021.111244.

[38] V.I. Pet'kov, A.S. Dmitrienko, M.V. Sukhanov, A.M. Koval'skii, E.Y. Borovikova, Synthesis, phase formation, and thermal expansion of sulfate phosphates with the $NaZr_2(PO_4)_3$ structure, Russ. J. Inorg. Chem. 61 (2016) 623–629, https://doi.org/10.1134/S0036023616050168.

[39] R.L. Frost, S.J. Palmer, A vibrational spectroscopic study of the mixed anion mineral sanjuanite $Al_2(PO_4)(SO_4)(OH)\cdot 9H_2O$, Spectrochim. Acta Part A Mol. Biomol. Spectrosc. 79 (2011) 1210–1214, https://doi.org/10.1016/j.saa.2011.04.044.

[40] M. Testa, V. La Parola, F. Mesrar, F. Ouanji, M. Kacimi, M. Ziyad, L. Liotta, Use of zirconium phosphate-sulphate as acid catalyst for synthesis of glycerol-based fuel additives, Catalysts 9 (2019) 148, https://doi.org/10.3390/catal9020148.

[41] K. Nakamoto, Infrared and Raman Spectra of Inorganic and Coordination Compounds, John Wiley & Sons, Inc., Hoboken, NJ, USA, 2008, https://doi.org/10.1002/9780470405840.

[42] J. Čejka, J. Sejkora, J. Plášil, S. Bahfenne, S.J. Palmer, R.L. Frost, A vibrational spectroscopic study of hydrated Fe^{3+} hydroxyl-sulfates; polymorphic minerals butlerite and parabutlerite, Spectrochim. Acta Part A Mol. Biomol. Spectrosc. 79 (2011) 1356–1363, https://doi.org/10.1016/j.saa.2011.04.069.

[43] H.H. Adler, P.F. Kerr, Variations in infrared spectra, molecular symmetry and site symmetry of sulfate minerals, Am. Mineral. 50 (1965) 132–147.

[44] V. Ivanovski, V.M. Petruševski, M.K. Gunde, The IR reflectance spectra of the $\nu_3(SO_4^{2-})$ and $\nu_4(SO_4^{2-})$ band regions of some Tutton salts using polarized radiation: testing the model dielectric function, Spectrochim. Acta Part A Mol. Biomol. Spectrosc. 61 (2005) 67–76, https://doi.org/10.1016/j.saa.2004.03.034.

[45] D.V. Deyneko, S.M. Aksenov, I. Nikiforov, S.Y. Stefanovich, B.I. Lazoryak, Symmetry inhomogeneity of $Ca_{9-x}Zn_xEu(PO_4)_7$ phosphor determined by second-harmonic generation and dielectric and photoluminescence spectroscopy, Cryst. Growth Des. (2020), 0c00637, https://doi.org/10.1021/acs.cgd.0c00637 acs.cgd.

[46] D.V. Deyneko, D.A. Spassky, V.A. Morozov, S.M. Aksenov, S.P. Kubrin, M. S. Molokeev, B.I. Lazoryak, Role of the Eu^{3+} distribution on the properties of β-$Ca_3(PO_4)_2$ phosphors: structural, luminescent, and ^{151}Eu Mössbauer spectroscopy study of $Ca_{9.5-1.5x}MgEu_x(PO_4)_7$, Inorg. Chem. 60 (2021) 3961–3971, https://doi.org/10.1021/acs.inorgchem.0c03813.

[47] B.I. Lazoryak, E.S. Zhukovskaya, O.V. Baryshnikova, A.A. Belik, O.N. Leonidova, D. V. Deyneko, A.E. Savon, N.G. Dorbakov, V.A. Morozov, Luminescence, structure and antiferroelectric-type phase transition in $Ca_8ZnEu(PO_4)_7$, Mater. Res. Bull. 104 (2018) 20–26, https://doi.org/10.1016/j.materresbull.2018.03.052.

[48] B.I. Lazoryak, V.A. Morozov, A.A. Belik, S.Y. Stefanovich, V.V. Grebenev, I. A. Leonidov, E.B. Mitberg, S.A. Davydov, O.I. Lebedev, G. Van Tendeloo, Ferroelectric phase transition in the whitlockite-type $Ca_9Fe(PO_4)_7$; Crystal structure of the paraelectric phase at 923 K, Solid State Sci. 6 (2004) 185–195, https://doi.org/10.1016/j.solidstatesciences.2003.12.007.

[49] G. Zhu, Z. Ci, Y. Shi, M. Que, Q. Wang, Y. Wang, Synthesis, crystal structure and luminescence characteristics of a novel red phosphor $Ca_{19}Mg_2(PO_4)_{14}$:Eu^{3+} for light emitting diodes and field emission displays, J. Mater. Chem. C. 1 (2013) 5960–5969, https://doi.org/10.1039/c3tc31263a.

[50] Y.Y. Dikhtyar, D.A. Spassky, V.A. Morozov, D.V. Deyneko, A.A. Belik, O. V. Baryshnikova, I.V. Nikiforov, B.I. Lazoryak, Site occupancy, luminescence and dielectric properties of β-$Ca_3(PO_4)_2$-type $Ca_8ZnLn(PO_4)_7$ host materials, J. Alloys Compd. (2022), 164521, https://doi.org/10.1016/j.jallcom.2022.164521.

[51] I.V. Nikiforov, D.V. Deyneko, D.A. Spassky, O.V. Baryshnikova, S.Y. Stefanovich, B. I. Lazoryak, Tunable luminescence and energy transfer in Eu^{3+} doped $Ca_8MTb(PO_4)_7$ (M = Mg, Zn, Ca) phosphors, Mater. Res. Bull. 130 (2020), 110925, https://doi.org/10.1016/j.materresbull.2020.110925.

[52] D.V. Deyneko, V.A. Morozov, E.S. Zhukovskaya, I.V. Nikiforov, D.A. Spassky, A. A. Belik, B.I. Lazoryak, The influence of second coordination-sphere interactions on the luminescent properties of β-$Ca_3(PO_4)_2$-related compounds, J. Alloys Compd. 815 (2020), 152352, https://doi.org/10.1016/j.jallcom.2019.152352.

[53] D. Zhang, X. Zhang, B. Zheng, Q. Sun, Z. Zheng, Z. Shi, Y. Song, H. Zou, Li^+ ion induced full visible emission in single Eu^{2+}-doped white emitting phosphor: Eu^{2+} site preference analysis, luminescence properties, and WLED applications, Adv. Opt. Mater. 9 (2021) 1–13, https://doi.org/10.1002/adom.202100337.

[54] M. Chen, Z. Xia, M.S. Molokeev, C.C. Lin, C. Su, Y.-C. Chuang, Q. Liu, C. Su, M. Chen, C.C. Lin, Q. Liu, M.S. Molokeev, Probing Eu^{2+} luminescence from different crystallographic sites in $Ca_{10}M(PO_4)_7$:Eu^{2+} (M = Li, Na, and K) with β-$Ca_3(PO_4)_2$-type structure, Chem. Mater. 29 (2017) 7563–7570, https://doi.org/10.1021/acs.chemmater.7b02724.

[55] R.A. Benhamou, A. Bessière, G. Wallez, B. Viana, M. Elaatmani, M. Daoud, A. Zegzouti, New insight in the structure-luminescence relationships of $Ca_9Eu(PO_4)_7$, J. Solid State Chem. 182 (2009) 2319–2325, https://doi.org/10.1016/j.jssc.2009.06.018.

[56] E. Antic-Fidancev, Simple way to test the validity of $^{2S+1}L_J$ Barycenters of Rare Earth Ions (e.g. $4f^2$, $4f^3$ and $4f^6$ Configurations), J. Alloys Compd. 300 (2000) 2–10, https://doi.org/10.1016/S0925-8388(99)00695-7.